J Mater Sci (2013) 48:4081–4087
DOI 10.1007/s10853-013-7220-1

Thermoelectric properties of p-type semiconductors copper chromium disulfide $CuCrS_{2+x}$

Cheng-Gong Han · Bo-Ping Zhang · Zhen-Hua Ge · Li-Juan Zhang · Yao-Chun Liu

Received: 10 December 2012 / Accepted: 4 February 2013 / Published online: 20 February 2013

Abstract A series of bulk samples $CuCrS_{2+x}$ ($x = 0$, 0.01, 0.02, 0.06, 0.10) were prepared by combining mechanical alloying and spark plasma sintering. The effect of excessive sulfur content on the phase structure, microstructure, and thermoelectric and optical properties was investigated. The excessive sulfur initially entered into the lattice sites and then into the lattice interstices. A direct band gap semiconductor for $CuCrS_2$ material with an optical band gap of about 2.48 eV was proved. An improved electrical conductivity 2980 S m^{-1} at 673 K reached along with an inversely varied Seebeck coefficient as increasing x value, which showed a maximum power factor of 104 μ W m^{-1} K^{-2} at 673 K for $CuCrS_{2.01}$ sample. In addition to the low thermal conductivity between 0.48 and 1.02 W m^{-1} K^{-1} in the whole temperature range, a peak ZT of 0.15 was achieved at 673 K for $CuCrS_{2.01}$ bulk sample, which was 36 % higher than that (0.11) of the $CuCrS_{2.00}$.

Introduction

Thermoelectric (TE) materials are widely used for both power generation and electronic refrigeration because of the directly convertible ability between electric and thermal energies [1]. The conversion efficiency of TE devices is related to the dimensionless figure merit (ZT), defined as $ZT = \alpha^2\sigma T/\kappa$, where α, σ, T, and κ are the Seebeck coefficient, electrical conductivity, absolute temperature, and thermal conductivity, respectively. Hence, the high-performance TE material requires high α, high σ, and low κ.

In recent years, intense efforts have been devoted to discovering new thermoelectric materials with multilayered structures due to the low lattice κ and the high α from the confinement of the electrons [2], such as $Bi_2Te_{2.7}Se_{0.3}$ [3], Bi_2S_3 [4], BiCuSeO [5, 6], and so on. Multilayered $CuCrS_2$ compound with a rhombohedral structure (space group R3m) was first prepared by Hahn through heating the binary chalcogenides [7]. It consists of series of alternating S–Cr–S triple layers perpendicular to the hexagonal c-axis along with an interlayer of copper atoms [8–10]. S atoms form a distorted cubic close packing, while Cr atoms occupy octahedral sites in the layer and Cu atoms occupy tetrahedral sites between the layers [11]. Since the adjacent trigonal layers are linked together by weak van der Waals force, the high mobility of Cu atoms is realized as raising the temperature, benefiting to improving σ and reducing κ. Lots of studies concerning $CuCrS_2$ have been done on the magnetic property [9–15] rather than the electronic transport property [15–19]. A preliminary σ research of single-crystal $CuCrS_2$ by Le Nagard et al. [15] indicated a semiconducting behavior along with low activation energy $E_{act} \approx 4$ meV and a large σ between 25.2 and 41.6 S cm^{-1} in the temperature range from 60 to 300 K. It was reported that the σ and α of $CuCrS_2$ semiconductor could be tailored from 0.75 to 2.00 S m^{-1} and −70 to 200 μ V K^{-1} via its non-stoichiometry controlling by varying sulfur vapor pressure during heating the $CuSO_4{\cdot}5H_2O$ and $Cr_2(SO_4)_3{\cdot}8H_2O$ in the N_2–H_2–H_2S gases between 873 and 1273 K [16]. A high σ 167 S cm^{-1} was attained at room temperature in the textured $CuCrS_2$ bulk prepared by solid-phase reaction sintered at 1123 K for 5 days [17]. The textured $CuCrS_2$ polycrystalline also showed an improved ZT from 0.4 to 0.9 at 300 K as prolonging reacting time from 2 to 8 days at 1173 K due to the

C.-G. Han · B.-P. Zhang (✉) · Z.-H. Ge · L.-J. Zhang · Y.-C. Liu
School of Materials Science and Engineering, University of Science and Technology Beijing, Beijing 100083, China
e-mail: bpzhang@ustb.edu.cn

increased Cr-vacancy disorder [18]. Similar to the $CuCrS_2$ with the same structure, the compounds $CuFeS_2$ [20] and $AgCrSe_2$ [19] showed *ZT* values 0.069 at 573 K and 0.4 at 798 K, respectively, which were all synthesized by spark plasma sintering (SPS) at different temperatures. The MA combining with SPS technique is known to be suitable to fabricate bulk materials with fine grains and dense microstructure, which is beneficial to improving TE properties. However, the TE property of $CuCrS_2$ compound prepared by MA and SPS was rarely studied so far. In our previous study, a low *ZT* value 0.11 was measured for $CuCrS_2$ bulk fabricated by MA and SPS due to its low σ 4.9 S cm^{-1} at 673 K [21]. σ was increased from 0.1 to 3.3 $\times$ 10^2 S cm^{-1} at 300 K as upping vanadium content from 0.3 to 0.9 via the carrier-doping effect in single-phase $CuCr_{1-x}V_xS_2$ [22]. The σ at 573 K in the n-type compound $CuFeS_{2-x}$ was also improved from 7.7 to 1.3 $\times$ 10^2 S cm^{-1} by increasing electron concentration, resulting in the improved *ZT* value from original 0.069 to 0.21 via decreasing sulfur content from 2 to 1.8 [20]. The σ value of the p-type semiconductor $CuAlS_{2+x}$ was improved from 0.9 to 4.6 Scm^{-1} by adding excessive sulfur content due to the increased holes concentration [23]. Therefore, the excellent TE transport properties are expectable for $CuCrS_2$ compound by optimizing the holes concentration via tailoring sulfur content in a non-stoichiometry. In the present work, bulk samples $CuCrS_{2+x}$ were prepared by MA and SPS technique. The phase structure, microstructure, and optical and TE properties were studied with a special emphasis on the effect of excessive sulfur content.

Experimental

Commercial powders of 99.9 % Cu, 99.9 % Cr, and 99.5 % S under the same 200 mesh were used as raw materials. Elemental powders with a chemical composition calculated by the molar ratio with a formula of $CuCrS_{2+x}$ ($x = 0$, 0.01, 0.02, 0.06, 0.10) were subjected to MA using a planetary ball mill (QM-4F, Nanjing University, China) at 425 rpm for 40 h in a purified argon atmosphere. The weight ratio of ball to powder was kept at 20:1. Bulk sample was synthesized under an axial compressive pressure of 40 MPa at 873 K by a SPS system (Sumitomo SPS1050, Japan) from the MA-treated powders. The heating rate and the holding time were 100 K min^{-1} and 5 min, respectively. The density of sintered samples was determined by the Archimedes method.

Phase structure was analyzed by X-ray diffraction (XRD, Cu Kα, BrukerD8, Germany). The fractograph was observed by a field emission scanning electron microscopy (FESEM, SUPRA^{TM} 55, Japan). The optical absorption was determined by the UV–vis spectrometry with an integrating sphere from 250 to 700 nm at room temperature (TU-1901, Purkinje General, Beijing). The α and σ values were measured from 323 to 673 K using a Seebeck coefficient/electrical conductivity measuring system (ZEM-2, Ulvac-Riko, Japan) in a helium atmosphere. The κ value was calculated by the relationship $\kappa = DC_pd$ from the thermal diffusivity (*D*) measured by the laser flash method (NETZSCH, LFA427, Germany), the specific heat capacity (C_p) with theoretical value calculated from the Dulong-Petit law and Cope's laws, and the density of sample (*d*).

Results and discussion

Figure 1 shows the XRD patterns of $CuCrS_{2+x}$ ($x = 0$, 0.01, 0.02, 0.06, 0.10) bulk samples with 2θ ranges 20°–80° (a) and 29.5°−30.5° (b). The diffraction peaks of $CuCrS_{2+x}$ ($x = 0$, 0.01, 0.02, 0.06) samples are well-matched with the pattern of the ternary $CuCrS_2$ (*PDF#65-2098*) without any detectable second phase, but an impurity phase $CuCr_2S_4$ (*PDF#65-4606*) is obviously indexed from the sample $CuCrS_{2.10}$. The 2θ angle of the (101) main diffraction peak for the bulk sample $CuCrS_{2.00}$ is about 29.93° and lower than that (30.00°) of the standard card ($CuCrS_2$, *PDF#65-2098*), which is usually found in the MA and/or SPS process owing to the loss and/or volatilization of sulfur [24]. If the lost sulfur was compensated by adding excessive sulfur, the position of the (101) peak should be reverted to the standard value (30.00°). However, the shifting trend for the (101) peak still continues to the low diffraction angle as increasing *x* over 0.02, which is centered at 29.84°, 29.79°, and 29.86° for the samples with $x = 0.01$, 0.02, and 0.06, and at 29.86° separated by XPS soft for the sample $CuCrS_{2.10}$, respectively. Hence, a real composition $CuCrS_{2.00}$ should exist between $x = 0$–0.01, associating with the reversion of the (101) peak to the standard value. On the other hand, when the *x* exceeds the balance composition to 0.01 and 0.02, the shifting trend to the low diffraction angle means that the excessive sulfur initially enters into the lattice sites and then into the interstitial sites, leading to the continuos enlargement of lattice constants for the samples $CuCrS_{2.01}$ and $CuCrS_{2.02}$. The position of the $CuCrS_2$ peaks reversely shifts to the high diffraction angle owing to the formation of sulfur-rich $CuCr_2S_4$ phase in the bulk samples $CuCrS_{2.10}$ and $CuCrS_{2.06}$ which is trace and detectable hardly by XRD in the later sample [25].

Figure 2a shows the lattice constants of $CuCrS_2$ phase for the bulk samples $CuCrS_{2+x}$ ($x = 0$, 0.01, 0.02, 0.06, 0.10) along with those of the polycrystalline [11] and standard ones. Inset shows a schematic sketch of the $CuCrS_2$ unit cell. The lattice parameters *a* and *b* of $CuCrS_2$ for all bulk samples are similar to those of the standard

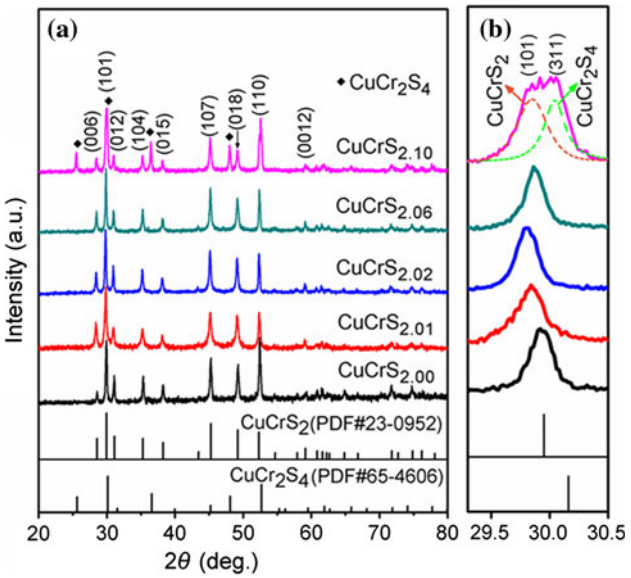

Fig. 1 XRD patterns of the $CuCrS_{2+x}$ ($x = 0$, 0.01, 0.02, 0.06, 0.10) bulk samples with 2θ ranges 20°–80° (**a**) and 29.5°–30.5° (**b**)

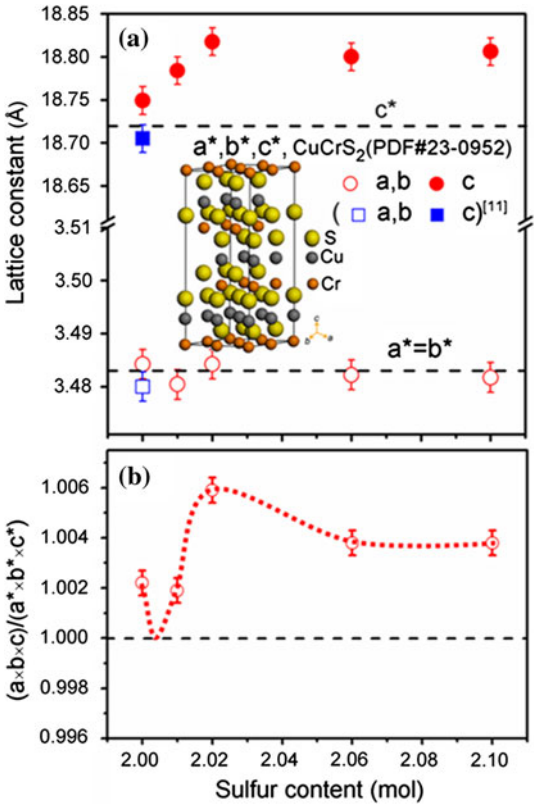

Fig. 2 **a** Lattice constants of the $CuCrS_{2+x}$ ($x = 0$, 0.01, 0.02, 0.06, 0.10) bulk samples along with that of the reported polycrystalline $CuCrS_2$ [11].*Inset* shows a schematic sketch of the $CuCrS_2$ unit cell. **b** Ratio of cell volume for $CuCrS_2$ between the bulk samples and the standard one

($CuCrS_2$, *PDF#23-0952*) and reported data, while the lattice parameter c is bigger than the standard one. The samples $CuCrS_{2.06}$ and $CuCrS_{2.10}$ show smaller lattice constants than the sample $CuCrS_{2.02}$, which is attributed to the presence of the $CuCr_2S_4$ phase. The ratio of cell volume between $CuCrS_2$ phase in the bulk sample and in the standard card (*PDF#23-0952*, a*, b*, and c*) shown in Fig. 2b exceeds 100 % (dash line) for all samples. The enlarged lattice is usually found in the MA and/or SPS process owing to the loss and/or volatilization of sulfur [24]. The sulfur-lack means a decrease in the number of ionic bond of S–Cu and/or S–Cr in the inset of Fig. 2a that favors a weakened gravitation between S layers and Cu and/or Cr layers, which contributes an enlarged lattice (Fig. 2b) especially in c-axis layer space (Fig. 2a). If the lost sulfur was compensated by upping x, the lattice size should be reverted to the standard one and the ratio of cell volume should become 100 %. However, this kind of situation is absent in our designed composition because of the wide interval. We infer that the change track on the ratio of cell volume should be like the dot line which has a turning point between $x = 0$–0.01. This consideration is also supported by the smaller cell volume for $CuCrS_{2.01}$ bulk sample than that for $CuCrS_{2.00}$ one. On the other hand, if the x exceeds this value, the excessive sulfur should enter into the interstitial sites. In a word, the excessive sulfur initially compensates the sulfur loss, corresponding to the fact that the cell volume returns to the dash line, and then the rest sulfur enters into the lattice interstices, leading to enlarging lattice parameters and increasing ratio of cell volume away from the dash line again. However, as $x \geq 0.06$, the appeared sulfur-rich $CuCr_2S_4$ second phase results in the slight decrease in lattices of main $CuCrS_2$ phase for $CuCrS_{2.06}$ and $CuCrS_{2.10}$ bulk samples. Hence, three equations related to the above behaviors about sulfur should be as follows:

$$CuCrS_{2-x} \rightarrow CuCrS_2 - xS \uparrow + xV_S^{\bullet\bullet} + 2xe' \quad (1)$$

$$CuCrS_{2+x} \rightarrow CuCrS_2 + xS_i'' + 2xh^{\bullet} \quad (2)$$

$$CuCrS_{2+x} \rightarrow yCuCr_2S_4 + Cu_{1-y}Cr_{1-2y}S_{2-4y+x} \quad (3)$$

Equation (1) indicates that the vacancy $V_S^{\bullet\bullet}$ and two electrons were generated if sulfur was lacking, while the interstitial solution S_i'' and two holes would be formed as shown in Eq. (2) if the sulfur entered into the interstitial sites. Equation (3) expresses that the sulfur content in the main phase $CuCrS_2$ would be deficient in a form of $Cu_{1-y}Cr_{1-2y}S_{2-4y+x}$ if the sulfur-rich $CuCr_2S_4$ phase appeared.

Figure 3 shows the FESEM micrographs of the fractured surfaces for the $CuCrS_{2+x}$ ($x = 0$, 0.01, 0.02, 0.06, 0.10) bulk samples, in which a layered microstructure with grain sizes ranging from 500 to 900 nm is noticed. An increased compactness in the micrographs for the bulk samples with increasing x from 0 to 0.02 is observed owing to the

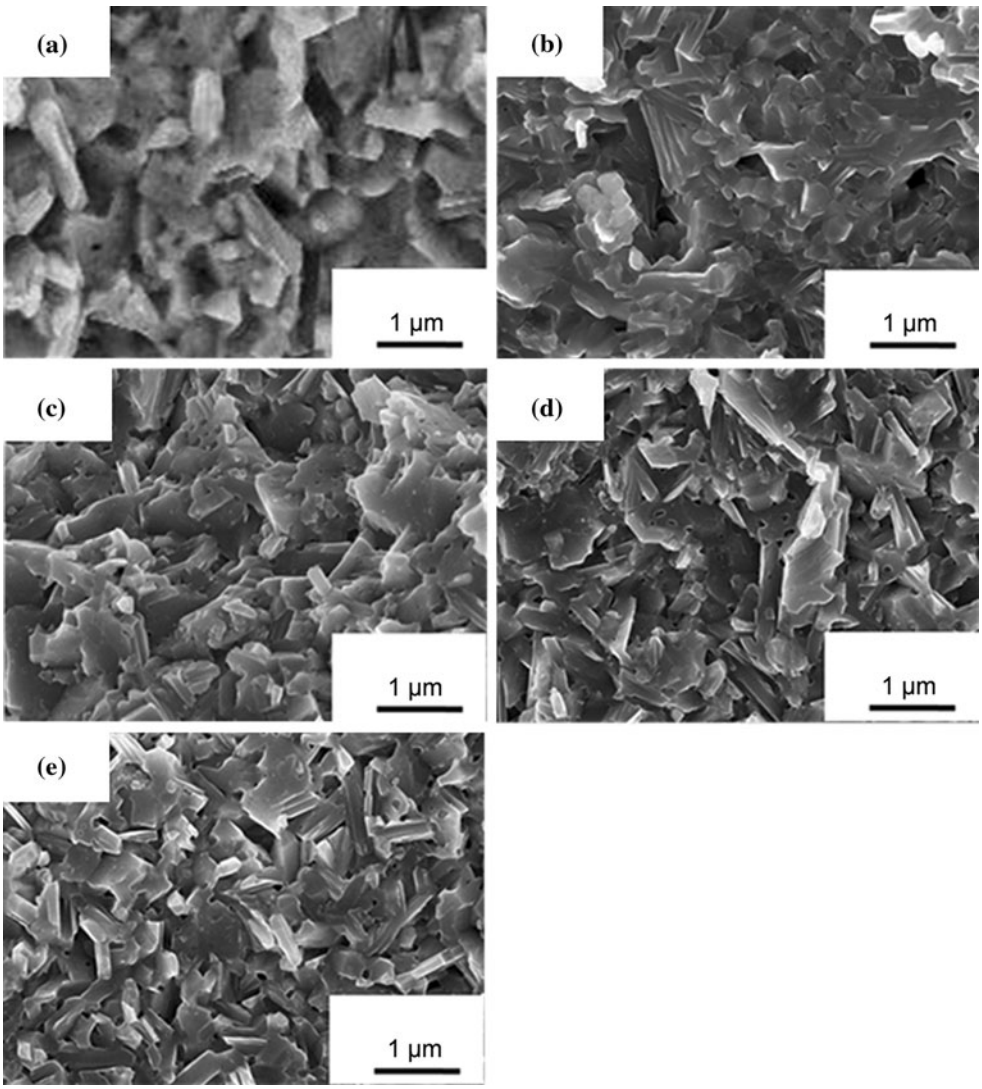

Fig. 3 FESEM micrographs of the fractured surfaces for bulk samples $CuCrS_{2.00}$ (**a**), $CuCrS_{2.01}$ (**b**), $CuCrS_{2.02}$ (**c**), $CuCrS_{2.06}$ (**d**), and $CuCrS_{2.10}$ (**e**)

interstitial solid of sulfur, along with an increased relative density from 94.6 to 95.2 and 98.4 %, while a decreasing trend appears with further increasing x due to the second phase.

Figure 4 shows the UV–vis absorption spectra of bulk samples $CuCrS_{2+x}$ ($x = 0$, 0.01, 0.02, 0.06, 0.10). All samples begin to absorb the incident light around 400 nm and show an obvious absorption peak at about 260 nm. The transition type of band gap semiconductor was determined from the following relation:

$$\alpha h\upsilon = A(E_g - h\upsilon)^n \quad (4)$$

where α, $h\upsilon$, A, and E_g is the absorption coefficient, the incident photon energy, the constant, and the optical band gap; and the exponent n for the direct and indirect transition is 1/2 and 2, respectively [26]. The plots of $(\alpha h\upsilon)^2$ or $(\alpha h\upsilon)^{1/2}$ versus $h\upsilon$ curve for all the bulk samples are shown in Fig. 5, in which the E_g was calculated by extrapolating the straight-line portion of this plot to the energy axis where $(\alpha h\upsilon)^2$ or $(\alpha h\upsilon)^{1/2} = 0$ [27–29]. As $n = 1/2$, the E_g in Fig. 5a was estimated to be 2.38–2.58 eV as in an inset of Fig. 5a, while the positive E_g is unobtainable by the same approach as $n = 2$ in Fig. 5b. It displays that $CuCrS_2$ is a direct band gap semiconductor rather than an indirect one.

Figure 6a shows the temperature dependence of the Seebeck coefficient (α) for $CuCrS_{2.00}$, $CuCrS_{2.01}$, $CuCrS_{2.02}$, and $CuCrS_{2.10}$ bulk samples, which is simply given as: $\alpha = \gamma - \ln n$, where γ and n are the scattering factor and carrier concentrations, respectively. The positive α indicates that all samples are p-type semiconductors. The α gradually increases with raising the measuring temperature and nearly

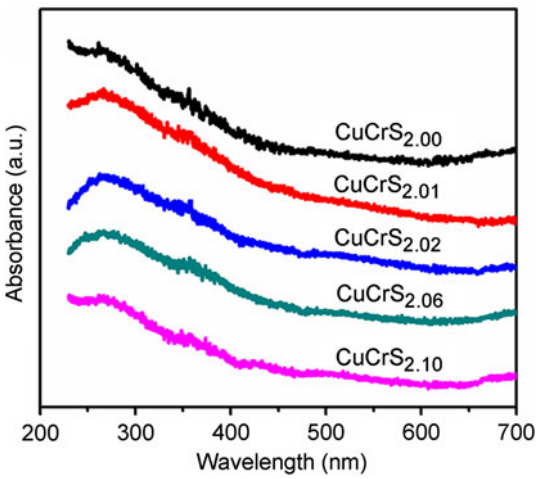

Fig. 4 UV–vis absorption spectra for $CuCrS_{2+x}$ ($x = 0$, 0.01, 0.02, 0.06, 0.10) bulk samples

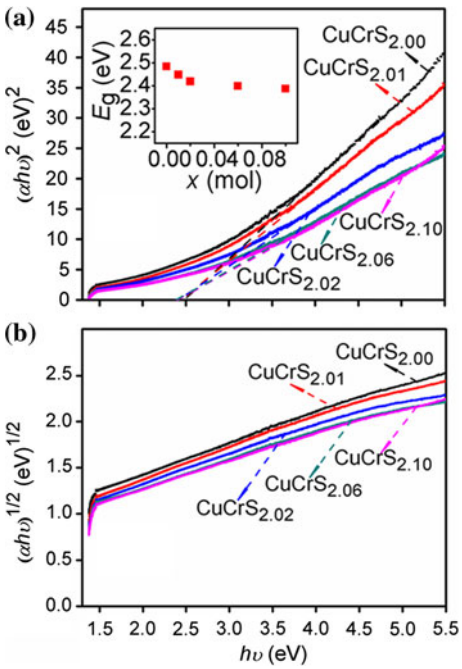

Fig. 5 A plot of $(\alpha h\upsilon)^n$ versus $h\upsilon$ for $CuCrS_{2+x}$ ($x = 0$, 0.01, 0.02, 0.06, 0.10) bulk samples. **a** $n = 2$ with the corresponding optical band gap in the *inset*, **b** $n = 1/2$

saturates at high temperature. This result is well similar to the varying trend on the Seebeck coefficient in the disordered phase of layered antiferromagnetic $CuCrS_2$ by Tewari et al. [17, 18, 30]. The measurement of magnetic moment of Cr atoms indicated that the rise of Seebeck coefficient with temperature in all the $CuCrS_2$ compounds was due to hopping conduction of polarons which might be due to the nonlocalized nature of their electrons, resulting from strong hybridization of the 3*d* orbital of Cr with the *sp* orbital of surrounding sulfur atoms. As shown in Eq. (2), adding excessive sulfur leads to formation of the interstitial solution,

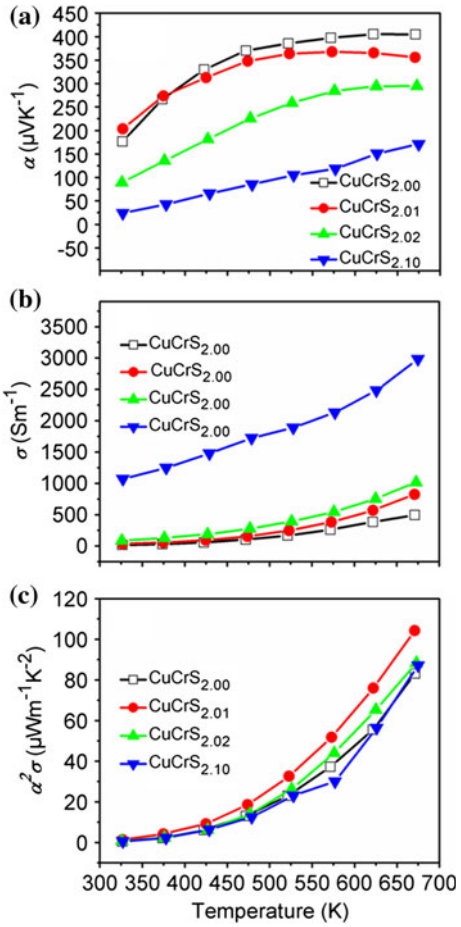

Fig. 6 Temperature dependence of Seebeck coefficient (**a**), electrical conductivity (**b**), and power factor (**c**) for $CuCrS_{2.00}$, $CuCrS_{2.01}$, $CuCrS_{2.02}$, and $CuCrS_{2.10}$ bulk samples

which produces two holes and effectively enhances the *n* of the p-type semiconductor $CuCrS_2$, resulting in the decreased α value among the whole temperature range. At the same time, the increased compactness with increasing *x* from 0 to 0.02 reduces γ which also impairs the α value [3]. The lowest α of $CuCrS_{2.10}$ in the whole temperature region ascribes the low α value 16 μ VK^{-1} at room temperature for $CuCr_2S_4$ prepared by solid-state reaction [31]. The $CuCrS_{2.00}$ sample reaches the largest α value, being 410 μ VK^{-1} at 673 K.

Figure 6b shows the temperature dependence of the electrical conductivity (σ) expressed as $\sigma = ne\mu$, where μ is the carrier mobility, for $CuCrS_{2.00}$, $CuCrS_{2.01}$, $CuCrS_{2.02}$, and $CuCrS_{2.10}$ bulk samples. All samples show a monotonous increase in the σ value with raising the measuring temperature from 323 to 673 K, displaying a typical semiconductor conducting behavior. The increased σ is due to the increased *n* and additionally accessorial conductivity of cationic Cu^+ for the superionic conductor $CuCrS_2$ as raising temperature [10, 32]. An increased σ appears as increasing *x* from 0 to 0.02 in the whole measuring temperature region, which is attributed to the increased *n* in Eq.

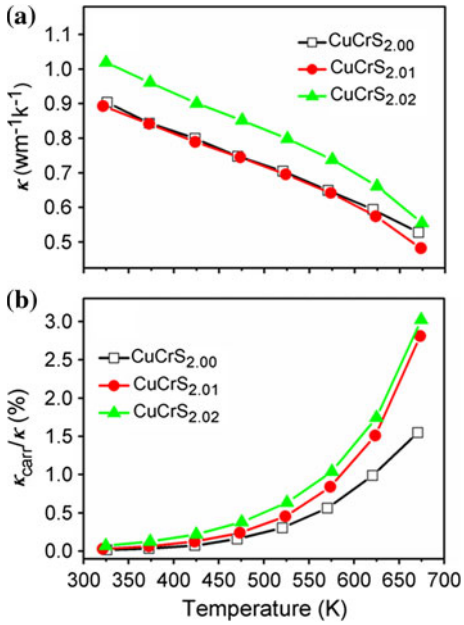

Fig. 7 Temperature dependence of thermal conductivity (**a**) and κ_{carr}/κ (**b**) for $CuCrS_{2.00}$, $CuCrS_{2.01}$, and $CuCrS_{2.02}$ bulk samples

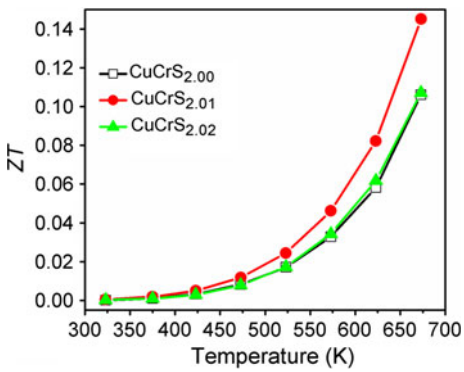

Fig. 8 Temperature dependence of *ZT* for $CuCrS_{2.00}$, $CuCrS_{2.01}$, and $CuCrS_{2.02}$ bulk samples

(2). The sample $CuCrS_{2.02}$ shows two times larger σ than the sample $CuCrS_{2.00}$, reaching a maximum value 1017 S m^{-1} at 673 K. The σ at room temperature is 17, 33, 87, and 1.07×10^3 S m^{-1} for the $CuCrS_{2.00}$, $CuCrS_{2.01}$, $CuCrS_{2.02}$, and $CuCrS_{2.10}$, respectively. Hence, the sharp increase of σ in $CuCrS_{2.10}$ is due to the presence of the metallic impurity $CuCr_2S_4$, which has a high σ of 1×10^5 S m^{-1} at room temperature [31, 33].

Figure 6c shows the temperature dependence of the power factor ($PF = \alpha^2\sigma$) for $CuCrS_{2.00}$, $CuCrS_{2.01}$, $CuCrS_{2.02}$, and $CuCrS_{2.10}$ samples. All samples show a monotonous increase in the PF with raising the temperature from 323 to 673 K. Among the whole temperature region, the PF of the bulk sample $CuCrS_{2.01}$ is the highest, reaching the maximum value 104 μ W m^{-1} K^{-2} at 673 K, which is attributed to the coupling effects of σ and α by optimizing S content.

Figure 7a shows the temperature dependence of the thermal conductivity (κ) for $CuCrS_{2.00}$, $CuCrS_{2.01}$, and $CuCrS_{2.02}$ bulk samples. The κ of all samples decreases with raising measuring temperature and maintains 0.48–1.02 W m^{-1} K^{-1}, which is lower than that of conventional TE bulk materials such as Bi_2Te_3 [3, 34] and SiGe [35, 36], owing to the lamellar structure of $CuCrS_2$ material [21]. A similar κ value is noticed in the samples $CuCrS_{2.00}$ and $CuCrS_{2.01}$ at 323–673 K, while an increased κ is seen in the sample $CuCrS_{2.02}$, which is ascribed to the effectively reduced grain boundary scattering from the increased density [37]. The κ consists of the lattice thermal conductivity ($\kappa_{lattice}$) and carrier thermal conductivity (κ_{carr}) calculated from the Wiedemann–Franz law [38]: $\kappa_{carr} = L\sigma T$, where L is the Lorenz number and approximately equals to 2.45×10^{-8} V^2 K^{-2}. As shown in Fig. 7b, the ratio value of κ_{carr}/κ in the temperature range from 323 to 673 K increases as upping x from 0 to 0.02, which is mainly due to the increased κ_{carr} related to the improved σ (Fig. 6b). The monotonously increased κ_{carr}/κ of bulk samples reaches only 1.5, 2.8, and 3.0 % at 673 K, respectively, indicating that $\kappa_{lattice}$ contributes mainly toward the overall κ. Consequently, the increased holes concentration by optimizing S content favors high σ and retains the low κ, which all contribute to the high *ZT* value. The figure of merit *ZT* in Fig. 8 shows a gradually increased trend as raising temperature for $CuCrS_{2.00}$, $CuCrS_{2.01}$, and $CuCrS_{2.02}$ samples and reaches the maximum value 0.15 at 673 K for the $CuCrS_{2.01}$, which is 36 % higher than that of the $CuCrS_{2.00}$.

Conclusions

$CuCrS_{2+x}$ ($x = 0$, 0.01, 0.02, 0.06, 0.10) bulk samples were fabricated by applying SPS techniques at 873 K using MA-treated powders. A direct band gap semiconductor of $CuCrS_2$ was concluded according to the UV–vis absorption spectra and the optical band gap was maintained at 2.38–2.48 eV for all samples. All samples are p-type semiconductors, which showed an obviously improved σ by adding excessive sulfur, thereby the maximum 1017 S m^{-1} at 673 K was achieved for single phase $CuCrS_{2.02}$, being two times larger than that of $CuCrS_{2.00}$ sample. The highest PF 104 μ W m^{-1} K^{-2} was obtained at 673 K for $CuCrS_{2.01}$ sample, which was 25 % higher than that of the counterpart $CuCrS_{2.00}$. The κ of samples varied between 0.48 and 1.02 W m^{-1} K^{-1}. The highest *ZT* value of 0.15 was achieved at 673 K in the present $CuCrS_{2.01}$ bulk sample, which was 36 % higher than that (0.11) of the $CuCrS_{2.00}$.

Acknowledgements This work was supported by National Natural Science Foundation of China (Grant No. 51272023), and High-Tech 973 Program of China (Grant No. 2013CB632503). We also appreciate the help provided by Prof. J.-F. Li's laboratory in Tsinghua University for part TE property measurements.

References

1. Li JF, Liu WS, Zhao LD, Zhou M (2010) NPG Asia Mater 2:152
2. Hicks LD, Dresselhaus MS (1993) Phys Rev B 47:12727
3. Yan X, Poudel B, Ma Y, Liu WS, Joshi G, Wang H, Lan YC, Wang DZ, Chen G, Ren ZF (2010) Nano Lett 10:3373
4. Ge ZH, Zhang BP, Yu ZX (2011) J Mater Res 26:2711
5. Liu Y, Zhao LD, Liu YC, Lan JL, Xu W, Li F, Zhang BP, Berardan D, Dragoe N, Lin YH, Nan CW, Li JF, Zhu H (2011) J Am Chem Soc 133:20112
6. Li F, Li JF, Zhao LD, Xiang K, Liu Y, Zhang BP, Lin YH, Nan CW, Zhu HM (2012) Energy Environ Sci 5:7188
7. Hahn H, de Lorent C (1957) Z Anorg Allg Chem 290:72
8. Al'mukhametov RF, Yakshibaev RA, Gabitov ÉV, Abdullin AR (2000) Phys Solid State 42:1508
9. Tsujii N, Kitazawa H (2007) J Phys Condens Matter 19:145245
10. Al'mukhametov RF, Yakshibaev RA, Gabitov ÉV (1999) Phys Solid State 41:1327
11. Abramova GM, Vorotynov AM, PetrakovskiÏ GA, Kiselev NI, Velikanov DA, Bovina AF, Al'mukhametov RF, Yakshibaev RA, Gabitov ÉV (2004) Phys Solid State 46:2225
12. Singh K, Maignan A, Martin C, Simon Ch (2009) Chem Mater 21:5007
13. Bongbrs IF, Van Bruggen CF, Koopstra J, Omloo WPFAM, Wiegers GA, Jellinek F (1968) J Phys Chem Solids 29:977
14. Abramova G, Pankrats A, Petrakovskii G, Rasch JCE, Boehm M, Vorotynov A, Tugarinov V, Szumszak R, Bovina A, Vasil'ev V (2009) Phys Rev B 80:104431
15. Le Nagard N, Collin G, Gorochov O (1979) Mater Res Bull 14:1411
16. Boutbila My A, Rasneur J, EI AatmaniM, Lyahyaoui H (1996) J Alloys Compd 244:23
17. Tewari GC, Tripathi TS, Rastogi AK (2010) J Electron Mater 39:1133
18. Tewari GC, Tripathi TS, Kumar P, Rastogi AK, Pasha SK, Gupta G (2011) J Electron Mater 40:2368
19. Gascoin F, Maignan A (2011) Chem Mater 23:2510
20. Li JH, Tan Q, Li JF (2013) J Alloys Compd 551:143
21. Chen YX, Zhang BP, Ge ZH, Shang PP (2012) J Solid State Chem 186:109
22. Tsujii N, Kitazawa H, Kido G (2006) Phys State Solidi 3:2775
23. Liu ML, Wang YM, Huang FQ, Chen LD, Wang WD (2007) Scr Mater 57:1133
24. Ge ZH, Zhang BP, Shang PP, Yu YQ, Chen C, Li JF (2011) J Electron Mater 40:1087
25. Ge ZH, Zhang BP, Liu Y, Li JF (2012) Phys Chem Chem Phys 14:4475
26. Pankove JI (1971) Optical processes in semiconductors. Prentice-Hall, Englewood Cliffs
27. Muthukumaran S, Gopalakrishnan R (2012) Physica B 407:3448
28. Singh G, Shrivastava SB, Jain D, Pandya S, Shripathi T, Ganesan V (2010) Bull Mater Sci 33:581
29. Wang SJ, Zhang BP, Yan LP, Deng W (2011) J Alloys Compd 509:5731
30. Tewari GC, Tripathi TS, Rastogi AK (2010) Z Kristallogr 225:471
31. Bouchard RJ, Russo PA, Wold A (1965) Inorg Chem 4:685
32. Yakshibaevg RA, Akmanovar GR, Almukhametov RF, Konev VN (1991) Phys Status Solidi A 124:417
33. Jeffrey Snyder G, Caillat T, Fleurial JP (2001) Mat Res Innovat 5:67
34. Zhang ZH, Sharma PA, Lavernia EJ, Yang N (2011) J Mater Res 26:475
35. Wang XW, Lee H, Lan YC, Zhu GH, Joshi G, Wang DZ, Yang J, Muto AJ, Tang MY, Klatsky J, Song S, Dresselhaus MS, Chen G, Ren ZF (2008) Appl Phys Lett 93:193121
36. Lee EK, Yin L, Lee YJ, Lee JW, Lee SJ, Lee J, Cha SN, Whang D, Hwang GS, Hippalgaonkar K, Majumdar A (2012) Nano Lett 12:2918
37. Fan XA, Yang JY, Chen RG, Yun HS, Zhu W, Bao SQ, Duan XK (2006) J Phys D 39:740
38. Hochbaum I, Chen R, Delgado RD, Liang WJ, Garnett EC, Najarian M, Majumdar A, Yang PD (2008) Nature 451:163